PERGAMON

International Journal of Solids and Structures 37 (2000) 7633–7654

INTERNATIONAL JOURNAL OF SOLIDS and STRUCTURES

www.elsevier.com/locate/ijsolstr

# Evaluation of nearly singular integrals in boundary element contour and node methods for three-dimensional linear elasticity

Subrata Mukherjee [a,*], Mandar K. Chati [a], Xiaolan Shi [b]

[a] *Department of Theoretical and Applied Mechanics, 212, Kimball Hall, Cornell Univeristy, Ithaca, NY 14853, 1503, USA*
[b] *DeHan Engineering Numerics, 95, Brown Road, Box 1016, Ithaca, NY 14850, USA*

Received 27 October 1999

**Abstract**

This article addresses the issue of nearly singular integrals that arise in boundary element methods (BEMS) when one tries to evaluate displacements and stresses at points inside a body that lie *close* to its bounding surface. An efficient new approach is proposed for the evaluation of these integrals. The same issue is then discussed in the context of the boundary contour method (BCM) and the boundary node method (BNM). Finally, numerical results, from both the BCM and the BNM, are presented for an illustrative problem. 

*Keywords:* Singular integrals; Boundary element; Linear elasticity

## 1. Introduction

### *1.1. Nearly singular integrals in the boundary element method*

It has been known in the boundary element method (BEM) community for many years, dating back atleast to Cruse (1969), that one experiences difficulties when trying to numerically evaluate variables of interest at a point inside a body $B$ that is *close* to its bounding surface $\partial B$. In three-dimensional (3-D) linear elasticity, for example, these difficulties arise when one tries to evaluate displacement components at such points, and such difficulties are usually compounded when one tries to evaluate the stress components there. The source of these difficulties is the fact that the traction kernel (in the standard displacement boundary integral equation (BIE)) becomes "nearly strongly singular" ($\mathcal{O}(1/r^2)$, where $r$ is the distance between an internal source point $p$ *close* to $\partial B$ and the nearest field point $Q$ on $\partial B$), while one of the kernels in the stress BIE becomes "nearly hypersingular" ($\mathcal{O}(1/r^3)$) as an internal point $p$ approaches the bounding surface $\partial B$.

BEM reserachers have proposed various numerical schemes for accurately computing such nearly singular integrals. Cruse and Aithal (1993) have proposed a semi-analytical approach using Taylor series

* Corresponding author. Tel.: +001-607-255-7143; fax: +001-607-255-2011.
*E-mail address:* sm85@cornell.edu (S. Mukherjee).

0020-7683/00/$ - see front matter 
PII: S0020-7683(99)00302-9

expansions for the kernels – with the singular part being integrated analytically and the remaining part computed using lower order Gaussian integration. Huang and Cruse (1993) present another approach involving a coordinate transformation that can smooth out the rapid variations of nearly singular kernels. Also, the above-referenced papers present comprehensive reviews of earlier work on the subject.

Other approaches include Gaussian integration with subdivisions (and usually many Gauss points), kernel cancellation methods (Nakagawa, 1993), the auxiliary surface of "tent" method (Lutz et al., 1992) first applied this idea to evaluate singular and nearly singular integrals; however, Liu et al. (1993) reported the need for excessive computational effort when applying this idea for evaluating nearly singular ones) and the line integral (Stoke regularization) method (Krishnasamy et al., 1994; Liu et al., 1993; Liu, 1998). A brief review of some of the above methods is available in Liu et al. (1993).

### *1.2. The line integral method*

This approach is considered by the authors of this article to be the most elegant one in the literature to date. The method is described very clearly, in detail, in Liu (1998). The basic idea is to convert the surface integral of the traction kernel, on a boundary element on which it becomes nearly singular, into a weakly singular surface integral, on that element, and a line integral around the bounding contour of that element. The solid angle term, which is a part of this integral, is also converted into a line integral. This procedure regularizes the integral, provided that the bounding countour of the surface element in question is chosen to be far from the internal point $p$ where the variable of interest needs to be evaluated. This approach is critical for solving BIEs in thin bodies and has been very successfully applied for solving such problems (e.g. Krishnasamy et al., 1994; Liu, 1998; Luo et al., 1998; Liu et al., 1999.)

### *1.3. Continuous boundary integral equations*

The line integral method described in the previous paragraph is excellent for accurately evaluating nearly singular integrals in thin structures. It is quite common, however, to encounter situations in which one has to evaluate displacements and stresses at internal points *close* to the boundary in bulky solid bodies. While the line integral method described above can also be used in such situations, a new method, which is *extremely easy* to implement in standard BEM codes, is described in this article. The current version of the new method is designed, as a post-processing step, for cases in which an evalaution point (at which one desires to determine the values of variables of interest) is an internal point that is close to the boundary of a bulky solid. It is currently not recommended for thin shell problems in which one typically encounters nearly singular integrals for evaluation points situated on the boundary of a body, when first setting up the BIE. It is felt, however, that the method presented in this article can be extended, in future, for use in thin shell problems.

The proposed method is based on continuous displacement and stress BIEs that already exist in the BEM literature (Cruse and Richardson, 1996). The reader is also referred to Rudolphi (1991) and Krishnasamy et al. (1992), where such ideas were first proposed in the context of Laplace's equation. These equations are called continuous because, under certain smoothness assumptions on the variables, their limits to the boundary (LTBs) exist. Typically, these equations have been used for the purpose of deriving regularized BIEs by taking such LTBs. In the present article, however, they are put to a novel and different use. Instead of taking LTBs, they are used directly to accurately evaluate nearly singular integrals that arise when the displacements and stresses (in linear elasticity) need to be evaluated at internal points that are *close* to the boundary of a bulky solid body. Details of the procedure are described later in this article.

The ideas described above are implemented in this article in the context of both the BCM and the BNM.

### 1.4. The boundary contour method

The usual BEM, for 3-D linear elasticity, requires numerical evaluations of surface integrals on boundary elements on the surface of a body (Mukherjee, 1982). Nagarajan et al. (1994, 1996) have recently proposed a novel appraoch, called the boundary contour method (BCM), that achieves a further reduction in dimension! The BCM, for 3-D linear elasticity problems, only requires numerical evaluation of line integrals over the closed bounding contours of the usual (surface) boundary elements.

The central idea of the BCM is the exploitation of the divergence-free property of the usual BEM integrand and a very useful application of Stokes' theorem, to analytically convert surface integrals on boundary elements to line integrals on closed contours that bound these elements. Lutz (1991) first proposed an application of this idea for the Laplace equation and Nagarajan et al. (1994) generalized this idea to linear elasticity. It is important to mention here that line integrals, evaluated in the 3-D BCM along opposite directions on a common line shared by contiguous boundary elements, are, as expected, equal and opposite. These integrals, however, must be separately evaluated in the BCM in order to obtain a system of linear algebraic equations that is necessary to solve for the boundary unknowns. Details are available in the BCM references cited in this article.

Numerical results for two-dimensional (2-D) problems, with linear boundary elements, are presented in Nagarajan et al. (1994) while results with quadratic boundary elements appear in Phan et al. (1997). The BCM for 3-D elasticity problems, with quadratic boundary elements, is presented in Nagarajan et al. (1996) and Mukherjee et al. (1997). Hypersingular boundary contour formulations, for 2-D (Phan et al., 1998) and 3-D (Mukherjee and Mukherjee, 1998) linear elasticity, have been proposed recently.

An interesting situation arises when one considers the evaluation of displacements and stresses in the BCM at internal points *close* to the boundary $\partial B$ of a bulky body $B$. The BCM has line integrals that are already "Stoke regularized", provided that the contours are far from the internal point in question! The BCM implementation described in the papers quoted in the above paragraph only involve line integrals, with the sole exception of the solid angle which is evaluated as a surface integral (for reasons that are described, for example, in Mukherjee and Mukherjee, 1998). Therefore, one way to evaluate nearly singular integrals in the BCM is to use the line integral formula (Eq. (16) Liu, 1998) for the solid angle . Another is to use boundary contour versions of the continuous BIEs mentioned above and still evaluate the solid angle as a surface integral. The second approach is described and implemented in this work.

### 1.5. The boundary node method

Mukherjee and Mukherjee (1997) have recently pioneered a breakthrough computational approach called the boundary node method (BNM) (Mukherjee and Mukherjee, 1997; Kothnur et al., 1999; Chati and Mukherjee, in press; Chati et al., 1999; Chati et al., 2000). This method is a combination of the moving least squared (MLS) interpolation scheme and the standard BIE method. The method divorces the traditional coupling between spatial discretization (meshing) and interpolation (as commonly practiced in the finite element method (FEM) or in the BEM). Instead, a "diffuse" interpolation, based on MLS interpolants, is used to represent the unknown functions; and surface cells, with a very flexible structure (e.g. any cell can be arbitrarily subdivided without affecting its neighbors) are used for integration (Figs. 1 and 2). Thus, the BNM retains the *meshless attribute of the MLS interpolants and the dimensionality advantage of the BEM.* As a consequence, the BNM only requires the specification of *points on the 2-D bounding surface* of a 3-D body, together with unstructured surface cells, thereby practically eliminating the meshing problem. In contrast, the FEM needs volume meshing, the BEM needs surface meshing, and the element-free Galerkin (EFG) method (see, e.g. Belytschko et al. (1996) for a recent overview) needs points throughout the domain of a body.

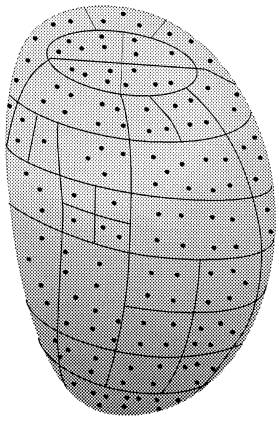

Fig. 1. BNM with nodes and cells.

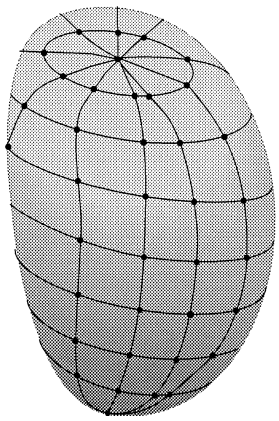

Fig. 2. BEM with nodes and elements.

It should be mentioned here that the discontinuous element BEM, in which the unknown functions are modeled as piecewise constant on elements, also allows an arbitrary subdivision of elements as illustrated in Fig. 1. Such an interpolation scheme, however, is not accurate and is not currently popular in solid mechanics analysis with the BEM. In contrast, the BNM truly divorces interpolation (carried out at nodal points) from discretization (cells are only required for integration). The diffuse interpolation scheme employed in the BNM is completely independent of the cell structure and the method allows a completely flexible cell structure as shown in Fig. 1. Thus, for example (as has been done in the present work), one can employ one node per cell in the BNM and still have a high order of interpolation of the boundary variables.

### *1.6. Outline of the present paper*

This article is organized as follows: The new idea, for regularizing nearly singular integrals in the BIEs for 3-D linear elasticity, is first presented for the BEM in Section 2. The matter of evaluation of dis-

placements, as well as stresses, at internal points that are close to the boundary of a body, are addressed here. This section is followed by descriptions of extensions of this idea to the BCM (Section 3) and to the BNM (Section 4). Section 5 presents numerical results for a selected problem – that of a sphere under internal pressure – using the BCM and BNM. A final section with concluding remarks completes this article.

It is of course well known that for all of these boundary based methods (BEM, BCM and BNM), the first step is to solve the primary boundary value problem (BVP) and obtain all the displacements and tractions on the surface of a body. This step is then followed by evaluation of displacements and stresses at points inside the body. *It is very important to state here that, in the interest of brevity, only the second step is discussed in this article.* The reader is referred to the references cited in the previous paragraphs, as well as, of course, books on the BEM (Mukherjee, 1982; Banerjee, 1994), for detailed discussions of procedures for solving the primary BVP by these boundary methods.

## 2. Nearly singular integrals in the BEM

### 2.1. Displacements at internal points close to the boundary

The starting point is the well-known BIE, for 3-D linear elasticity, at an internal point $p$ in a body $B$ (Rizzo, 1967):

$$u_k(p) = \int_{\partial B} [U_{ik}(p,Q)\sigma_{ij}(Q) - \Sigma_{ijk}(p,Q)u_i(Q)]n_j(Q)\,\mathrm{d}S(Q). \tag{1}$$

Here, $\partial B$ is the bounding surface of a body $B$ with infinitesimal surface area $\mathrm{d}\mathbf{S} = \mathrm{d}S\mathbf{n}$, where $\mathbf{n}$ is the unit outward normal to $\partial B$ at a point on it. The stress tensor is $\boldsymbol{\sigma}$ and the displacement vector is $\mathbf{u}$. A source point is denoted as $p$ (or $P$) and a field point as $q$ (or $Q$) (Upper case letters denote points on $\partial B$ while lower case letters denote points inside $B$.) The BEM Kelvin kernels $\mathbf{U}$ and $\boldsymbol{\Sigma}$ are available in many referenes. They are given in Appendix A for completeness.

Alternatively, one can write Eq. (1) in terms of the traction $\boldsymbol{\tau} = \boldsymbol{\sigma}\cdot\mathbf{n}$ and traction kernel $\mathbf{T}$ as:

$$u_k(p) = \int_{\partial B} [U_{ik}(p,Q)\tau_i(Q) - T_{ik}(p,Q)u_i(Q)]\,\mathrm{d}S(Q). \tag{2}$$

The new kernel $\mathbf{T}$ is also given in Appendix A.

A continuous version of Eq. (1) is available in the literature (Cruse and Richardson, 1996). This equation has the form:

$$u_k(p) = u_k(\hat{P}) + \int_{\partial B} [U_{ik}(p,Q)\sigma_{ij}(Q) - \Sigma_{ijk}(p,Q)\{u_i(Q) - u_i(\hat{P})\}]n_j(Q)\,\mathrm{d}S(Q), \tag{3}$$

where $p \in B$ is now an internal point *close* to $\partial B$ and a target point $\hat{P} \in \partial B$ is *close* to the point $p$ (see Fig. 3). An alternative form of Eq. (3) is:

$$u_k(p) = u_k(\hat{P}) + \int_{\partial B} [U_{ik}(p,Q)\tau_i(Q) - T_{ik}(p,Q)\{u_i(Q) - u_i(\hat{P})\}]\,\mathrm{d}S(Q). \tag{4}$$

Eq. (3) or Eq. (4) is called "continuous" since it has a continuous limit to the boundary (LTB as $p \to \hat{P} \in \partial B$) provided that $u_i(Q) \in C^{0,\alpha}$ (i.e., Hölder continuous). Taking this limit is the standard approach for obtaining the well-known regularized form of Eq. (1):

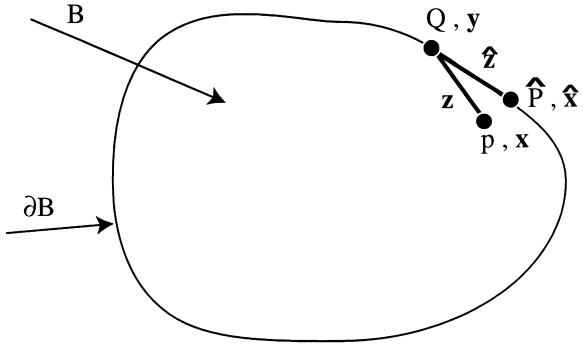


Fig. 3. A body with source point $p$, field point $Q$ and target point $\hat{P}$.

$$0 = \int_{\partial B} [U_{ik}(P,Q)\sigma_{ij}(Q) - \Sigma_{ijk}(P,Q)\{u_i(Q) - u_i(P)\}]n_j(Q)\,\mathrm{d}S(Q), \tag{5}$$

where, in keeping with standard notation, the target point $\hat{P}$ has been replaced by a generic boundary point $P$.

In this work, however, Eq. (3) or Eq. (4) is put to a different, and novel use. It is first observed that $T_{ik}$ in Eq. (4) is $\mathcal{O}(1/r^2(p,Q))$ as $Q \to p$, whereas $\{u_i(Q) - u_i(\hat{P})\}$ is $\mathcal{O}(r(\hat{P},Q))$ as $Q \to \hat{P}$. Therefore, as $Q \to \hat{P}$, the product $T_{ik}(p,Q)\{u_i(Q) - u_i(\hat{P})\}$, which is $\mathcal{O}(r(\hat{P},Q)/r^2(p,Q)), \to 0$! As a result, Eq. (4) or Eq. (3) can be used to easily and accurately evaluate the displacement components $u_k(p)$ for $p \in B$ close to $\partial B$. *This idea is the main contribution of this article*.

It is noted here that while it is usual to use Eq. (1) or Eq. (2) to evaluate $u_k(p)$ when $p$ is *far* from $\partial B$, Eq. (3) or Eq. (4) is also valid in this case (the target point $\hat{P}$ can be chosen as *any* point on $\partial B$ when $p$ is far from $\partial B$). Therefore, it is advisable to use the continuous Eq. (3) or Eq. (4) universally for all points $p \in B$. This procedure would eliminate the need to classify, apriori, whether $p$ is near to, or far from $\partial B$.

### 2.2. Displacement gradients and stresses at internal points close to the boundary

The BIE (Eq. (1)) can be differentiated with respect to $x_n(p)$ to give:

$$u_{k,n}(p) = -\int_{\partial B} [U_{ik,n}(p,Q)\sigma_{ij}(Q) - \Sigma_{ijk,n}(p,Q)u_i(Q)]n_j(Q)\,\mathrm{d}S(Q). \tag{6}$$

Please note that the negative sign in the right hand side of Eq. (6) arises from the fact that, following usual convention, the kernel derivatives are written with respect to field point coordinates $y_n(q)$. (In the rest of this paper, a source point $p$ (or $P$) has coordinates $\mathbf{x}$, the target point $\hat{P}$ has coordinates $\hat{\mathbf{x}}$ and a field point $q$ (or $Q$) has coordinates $\mathbf{y}$.)

An alternative form of Eq. (6), using Hooke's law, becomes:

$$\sigma_{ij}(p) = \int_{\partial B} [D_{ijk}(p,Q)\tau_k(Q) - S_{ijk}(p,Q)u_k(Q)]\,\mathrm{d}S_Q. \tag{7}$$

The new kernels **D** and **S** are available in many references. They are given in Appendix A for completeness of this article.

Continuous versions of Eqs. (6) and (7) can be written as (Cruse and Richardson, 1996):

$$u_{k,n}(p) = u_{k,n}(\hat{P}) - \int_{\partial B} U_{ik,n}(p,Q)[\sigma_{ij}(Q) - \sigma_{ij}(\hat{P})]n_j(Q)\,\mathrm{d}S(Q) + \int_{\partial B} \Sigma_{ijk,n}(p,Q)[u_i(Q) - u_i(\hat{P}) - u_{i,\ell}(\hat{P})(y_\ell(Q) - x_\ell(\hat{P}))]n_j(Q)\,\mathrm{d}S(Q), \tag{8}$$

$$\sigma_{ij}(p) = \sigma_{ij}(\hat{P}) + \int_{\partial B} D_{ijk}(p,Q)[\tau_k(Q) - \sigma_{km}(\hat{P})n_m(Q)]\,\mathrm{d}S(Q) - \int_{\partial B} S_{ijk}(p,Q)[u_k(Q) - u_k(\hat{P}) - u_{k,\ell}(\hat{P})(y_\ell(Q) - x_\ell(\hat{P}))]\,\mathrm{d}S(Q). \tag{9}$$

This time, the integrands in Eq. (8) or Eq. (9) are $\mathcal{O}(r(\hat{P},Q)/r^2(p,Q))$ and $\mathcal{O}(r^2(\hat{P},Q)/r^3(p,Q))$ as $Q \to \hat{P}$. As for the continuous BIEs in the previous section, the integrands in Eqs. (8) and (9) $\to 0$ as $Q \to \hat{P}$. Either of these equations, therefore, are very useful for evaluating the stresses at an internal point $p$ that is *close* to $\partial B$. Of course (please see the discussion regarding displacements in the previous section), they can also be conveniently used to evaluate stresses at *any* point $p \in B$.

Henceforth, the use of Eqs. (1), (2), (6) or (7) will be referred to as the *standard method*, while use of Eqs. (3), (4), (8) or Eq. (9) will be referred to as the *new method*.

## 3. Nearly singular integrals in the BCM

### 3.1. Displacements at internal points

A brief summary of the BCM is presented below. The reader is referred to, for example, Mukherjee et al. (1997) or Mukherjee and Mukherjee (1998) for a detailed description of the method.

The first step is to write Eq. (1) as:

$$u_k(\mathbf{x}) = \int_{\partial B} [U_{ik}(\mathbf{x},\mathbf{y})\sigma_{ij}(\mathbf{y}) - \Sigma_{ijk}(\mathbf{x},\mathbf{y})u_i(\mathbf{y})]\mathbf{e}_j \cdot \mathrm{d}\mathbf{S}(\mathbf{y}) \equiv \int_{\partial \mathbf{B}} \mathbf{F_k} \cdot \mathrm{d}\mathbf{S}(\mathbf{y}), \tag{10}$$

where $\mathbf{e}_j, j = 1,2,3$ are global Cartesian unit vectors.

It has been shown (Nagarajan et al., 1994, 1996; Mukherjee et al., 1997) that the integrand vector $\mathbf{F}_k$ in Eq. (10) is divergence-free and that the surface integral in it, over an open surface patch $S \in \partial B$, can be converted to a contour integral around the bounding curve $C$ of $S$, by applying Stokes' theorem. Therefore, vectors $\mathbf{V}_k$ exist such that:

$$\int_S \mathbf{F}_k \cdot \mathrm{d}\mathbf{S} = \oint_C \mathbf{V}_k \cdot \mathrm{d}\mathbf{r}. \tag{11}$$

As the vectors $\mathbf{F}_k$ contain the unknown fields $\mathbf{u}$ and $\boldsymbol{\sigma}$, shape functions must be chosen for these variables, and potential functions derived for each linearly independent shape function, in order to determine the vectors $\mathbf{V}_k$. Also, since the kernels in Eq. (10) are functions only of $z_k = y_k(Q) - x_k(P)$ (and not of the source and field coordinates separately), these shape functions must also be written in the coordinates $z_k$ in order to determine the potential vectors $\mathbf{V}_k$. Finally, these shape functions are global in nature and are chosen to satisfy, a priori, the Navier–Cauchy equations of equilibrium. The weights, in linear combinations of these shape functions, however, are defined piecewise on boundary elements.

Quadratic shape functions are used in this work. One has, on a boundary element,

$$i = \sum_{\alpha=1}^{27} \beta_\alpha \overline{u}_{\alpha i}(y_k) = \sum_{\alpha=1}^{27} \hat{\beta}_\alpha(x_k)\overline{u}_{\alpha i}(z_k), \tag{12}$$

$$\Sigma_{ij} = \sum_{\alpha=1}^{27} \beta_\alpha \overline{\sigma}_{\alpha ij}(y_k) = \sum_{\alpha=1}^{27} \hat{\beta}_\alpha(x_k)\overline{\sigma}_{\alpha ij}(z_k), \tag{13}$$

where $\overline{u}_{\alpha i}, \overline{\sigma}_{\alpha ij}$ (with $i, j = 1, 2, 3$ and $\alpha = 1, 2, \ldots, 27$) are the shape functions and $\beta_\alpha$ are the weights in the linear combinations of the shape functions. Each boundary element has, associated with it, 27 constants $\beta_\alpha$ which will be related to physical variables on that element. This set of $\beta$'s differ from one element to the next.

The displacement shape functions for $\alpha = 1, 2, 3$ are constants, those for $\alpha = 4, \ldots, 12$ are of the first degree and those for $\alpha = 13, \ldots, 27$ are of the second degree. There are a total of 27 linearly independent (vector) shape functions $\overline{\mathbf{U}}_\alpha$. The shape functions for the stresses are obtained from those for the displacements through the use of Hooke's law. The shape functions $\overline{u}_{\alpha i}$ and $\overline{\sigma}_{\alpha ij}$ are given in Mukherjee et al. (1997).

It is easy to show that the coordinate transformation $z_k = y_k - x_k\,(k = 1, 2, 3)$, results in the constants $\hat{\beta}_j$ being related to the $\beta_\alpha$'s as follows:

$$\hat{\beta}_i(x_k) = \sum_{\alpha=1}^{27} S_{i\alpha}(x_k)\beta_\alpha, \quad i = 1, 2, 3, \tag{14}$$

$$\hat{\beta}_k(x_m) = \sum_{\alpha=1}^{27} R_{n\alpha}(x_m)\beta_\alpha, \quad k = 4, 5, \ldots, 12, \quad n = k - 3, \tag{15}$$

$$\hat{\beta}_\alpha = \beta_\alpha, \quad \alpha = 13, 14, \ldots, 27, \tag{16}$$

where

$$S_{i\alpha}(x_k) = \overline{u}_{\alpha i}(x_k), \quad i = 1, 2, 3, \qquad \alpha = 1, 2, \ldots, 27,$$

$$R_{k\alpha}(x_m) = \left.\frac{\partial \overline{u}_{\alpha\ell}(y_m)}{\partial y_j}\right|_{x_m}, \quad k = 1, 2, \ldots, 9, \qquad \alpha = 1, 2, \ldots, 27$$

with $j = 1 + \lfloor (k-1)/3 \rfloor$ and $\ell = k - 3j + 3$. Here, the symbol $\lfloor n \rfloor$, called the floor of $n$, denotes the largest integer less than or equal to $n$.

It is useful to note that the matrices $\mathbf{S}$ and $\mathbf{R}$ are functions of only the source point coordinates $(x_1, x_2, x_3)$.

The procedure for designing boundary elements in the 3-D BCM is discussed in detail in Nagarajan et al. (1996) and Mukherjee et al. (1997) . A set of primary physical variables $a_k$, whose number must match the number (here 27) of artificial variables $\beta_k$ on a boundary element, are chosen first. A square invertible transformation matrix $\mathbf{T}$ relates the vectors $\mathbf{a}$ and $\beta$ on a boundary element $m$ according to the equation:

$$\overset{m}{a} = \overset{m}{T}\beta. \tag{17}$$

Finally, Eq. (1) can be shown to have the boundary contour version (Mukherjee et al., in press):

$$\begin{aligned} u_k(\mathbf{x}) = {} & \frac{1}{2}\sum_{m=1}^{M}\sum_{\alpha=13}^{27}\left[\oint_{Lm} (\overline{\sigma}_{\alpha ij}(\mathbf{z})U_{ik}(\mathbf{z}) - \overline{u}_{\alpha i}(\mathbf{z})\Sigma_{ijk}(\mathbf{z}))\epsilon_{jnt} z_n \,\mathrm{d}z_t\right]\left[\overset{m}{T^{-1}}\overset{m}{a}\right]_\alpha \\ & + \sum_{m=1}^{M}\sum_{\alpha=14}^{12}\left[\oint_{Lm} (\overline{\sigma}_{\alpha ij}(\mathbf{z})U_{ik}(\mathbf{z}) - \overline{u}_{\alpha i}(\mathbf{z})\Sigma_{ijk}(\mathbf{z}))\epsilon_{jnt} z_n \,\mathrm{d}z_t\right]\left[R(p)\overset{m}{T^{-1}}\overset{m}{a}\right]_{\alpha-3} \\ & + \sum_{m=1}^{M}\sum_{\alpha=1}^{3}\left[\oint_{Lm} D_{\alpha jk}(\mathbf{z})\,\mathrm{d}z_j\right]\left[S(p)\overset{m}{T^{-1}}\overset{m}{a}\right]_\alpha \end{aligned} \tag{18}$$

with

$$\oint_{Lm} D_{\alpha jk}\,\mathrm{d}x_j = -\int_{Sm} \Sigma_{\alpha jk}\mathbf{e}_j\cdot\mathrm{d}\mathbf{S} = \frac{1}{8\pi(1-\nu)}\oint_{Lm}\epsilon_{kij}\frac{r_{,\alpha}\,r_{,i}}{r}\,\mathrm{d}x_j + \frac{1-2\nu}{8\pi(1-\nu)}\oint_{Lm}\epsilon_{\alpha kj}\frac{1}{r}\,\mathrm{d}x_j + \frac{\Theta}{4\pi}\delta_{\alpha k}. \tag{19}$$

Here $L_m$ is the bounding contour of the surface element $S_m$. In the above, $\Theta$ is the solid angle (subtended by a surface element $m$ at a collocation point $P$), which is defined as

$$\Theta = \int_{Sm}\frac{\mathbf{r}\cdot\mathrm{d}\mathbf{S}}{r^3}. \tag{20}$$

Also, $\overset{m}{T}$ and $\overset{m}{a}$ are the transformation matrix and primary physical variable vectors, respectively, on element $m$, and $\epsilon_{ijk}$ is the usual alternating symbol.

The surface integral formula (20), is very easy to implement in a computer code, and has been usesd to obtain the numerical results reported in this article. Please note that the solid angle calculation from Eq. (20) is purely geometrical and does not involve any physical variables. This is the only time that a surface integral is evaluated in the BCM.

### 3.2. Displacements at internal points close to the boundary

The first step is to choose the target point $\hat{P}$ at or close to the centroid of a boundary element. Since all other terms in Eq. (18), except the solid angle, are evaluated as contour integrals, these terms are already regularized. There are atleast two ways of regularizing the solid angle term in Eq. (18). The first is to evaluate the solid angle $\Theta$ (see Eq. (20)) as a line integral by employing Eq. (16) of Liu (1998) . The second is to use a boundary contour version of Eq. (3) and still evaluate $\Theta$ as a surface integral. The latter approach is adopted in this work.

The boundary contour version of Eq. (3) can be obtained easily. This equation is

$$\begin{aligned} u_k(p) = u_k(\hat{P}) &+ \frac{1}{2}\sum_{m=1}^{M}\sum_{\alpha=13}^{27}\left[\oint_{Lm}(\overline{\sigma}_{\alpha ij}(\mathbf{z})U_{ik}(\mathbf{z}) - \overline{u}_{\alpha i}(\mathbf{z})\Sigma_{ijk}(\mathbf{z}))\epsilon_{jst}z_s\,\mathrm{d}z_t\right]\left[\overset{m}{T^{-1}}\overset{m}{a}\right]_{\alpha} \\ &+ \sum_{m=1}^{M}\sum_{\alpha=4}^{12}\left[\oint_{Lm}(\overline{\sigma}_{\alpha ij}(\mathbf{z})U_{ik}(\mathbf{z}) - \overline{u}_{\alpha i}(\mathbf{z})\Sigma_{ijk}(\mathbf{z}))\epsilon_{jst}z_s\,\mathrm{d}z_t\right]\left[R(p)\overset{m}{T^{-1}}\overset{m}{a}\right]_{\alpha-3} \\ &+ \sum_{m=1}^{M}\sum_{\alpha=1}^{3}\left[\oint_{Lm}D_{\alpha jk}(\mathbf{z})\,\mathrm{d}z_j\right]\left[S(p)\overset{m}{T^{-1}}\overset{m}{a} - S(\hat{P})\beta^{\hat{P}}\right]_{\alpha}, \end{aligned} \tag{21}$$

where

$$u_k(\hat{P}) = \hat{\beta}_k^{\hat{P}} = \sum_{\alpha=1}^{27}S_{k\alpha}(\hat{P})\beta_{\alpha}^{\hat{P}}. \tag{22}$$

It is important to note that, on a singular element (i.e., when integration is being carried out on an element that contains the point $\hat{P}$) one has:

$$\overset{m}{T^{-1}}\overset{m}{a} = \overset{m}{\beta} = \beta^{\hat{P}}. \tag{23}$$

In this case, the numerator of the last integrand in Eq. (21) is $\mathcal{O}(r(p,\hat{P}))$, whereas the denominator in the solid angle term is $\mathcal{O}(r^2(p,\hat{P}))$ as $Q \to \hat{P}$, so that Eq. (21) is "nearly weakly singular" as $Q \to \hat{P}$. It is useful to remember that the integral of $D_{\alpha jk}$ in Eq. (21) contains the solid angle term which is evaluated as a surface integral.

### 3.3. Displacement gradients at internal points

The boundary contour version of Eq. (6) has been derived before (Mukherjee and Mukherjee, 1998). This equation is:

$$\begin{aligned}
u_{k,n}(\mathbf{x}) = & -\sum_{m=1}^{M}\sum_{\alpha=13}^{27}\left[\oint_{Lm}(\overline{\sigma}_{\alpha ij}(\mathbf{z})U_{ik}(\mathbf{z}) - \overline{u}_{\alpha i}(\mathbf{z})\Sigma_{ijk}(\mathbf{z}))\epsilon_{jnt}\,\mathrm{d}z_t\right]\left[\overset{m}{T}{}^{-1}\overset{m}{a}\right]_{\alpha} \\
& +\sum_{m=1}^{M}\sum_{\alpha=4}^{12}\left[\oint_{Lm}(\overline{\sigma}_{\alpha ij}(\mathbf{z})U_{ik}(\mathbf{z})\overline{u}_{\alpha i}(\mathbf{z})\Sigma_{ijk}(\mathbf{z}))\epsilon_{jst}z_s\,\mathrm{d}z_t\right]\left[R_{,n}(p)\overset{m}{T}{}^{-1}\overset{m}{a}\right]_{\alpha-3} \\
& -\sum_{m=1}^{M}\sum_{\alpha=4}^{12}\left[\oint_{Lm}(\overline{\sigma}_{\alpha ij}(\mathbf{z})U_{ik}(\mathbf{z}) - \overline{u}_{\alpha i}(\mathbf{z})\Sigma_{ijk}(\mathbf{z}))\epsilon_{jnt}\,\mathrm{d}z_t\right]\left[R(p)\overset{m}{T}{}^{-1}\overset{m}{a}\right]_{\alpha-3} \\
& +\sum_{m=1}^{M}\sum_{\alpha=1}^{3}\left[\oint_{Lm}D_{\alpha jk}(\mathbf{z})\,\mathrm{d}z_j\right]\left[S_{,n}(p)\overset{m}{T}{}^{-1}\overset{m}{a}\right]_{\alpha} \\
& +\sum_{m=1}^{M}\sum_{\alpha=1}^{3}\left[\oint_{Lm}\Sigma_{\alpha jk}(\mathbf{z})\epsilon_{jnt}\,\mathrm{d}z_j\right]\left[S(p)\overset{m}{T}{}^{-1}\overset{m}{a}\right]_{\alpha}. \qquad (24)
\end{aligned}$$

### 3.4. Displacement gradients at internal points close to the boundary

As before, for the case of displacement evaluation at an internal point close to the boundary of a body (see start of Section 3.2), one has two choices with respect to the strategy for evaluation of the solid angle. Again, for the sake of uniformity, a boundary contour version of Eq. (8) is used here, together with evaluation of the solid angle as a surface integral.

A boundary contour version of Eq. (8) is obtained in a manner that is quite analogous to the approach discussed in Mukherjee and Mukherjee (1998). The first step is to use the product rule to transform Eq. (8) to the form:

$$\begin{aligned}
u_{k,n}(p) = u_{k,n}(\hat{P}) & - \int_{\partial B}\left[U_{ik}(p,Q)\left[\sigma_{ij}(Q) - \sigma_{ij}(\hat{P})\right] - \Sigma_{ijk}(p,Q)\left[u_i(Q) - u_i^{(L)}\right]\right]_{,n} n_j(Q)\,\mathrm{d}S(Q) \\
& + \int_{\partial B}\left[U_{ik}(p,Q)\sigma_{ij,n}(Q) - \Sigma_{ijk}(p,Q)\left[u_{i,n}(Q) - u_{i,n}(\hat{P})\right]\right]n_j(Q)\,\mathrm{d}S(Q), \qquad (25)
\end{aligned}$$

where (see Fig. 3)

$$u_i^{(L)} = u_i(\hat{P}) - u_{i,\ell}(\hat{P})\hat{z}_\ell \qquad (26)$$

with

$$\hat{z}_\ell = y_\ell(Q) - x_\ell(\hat{P}) \equiv y_\ell - \hat{x}_\ell. \qquad (27)$$

The BCM version of Eq. (8) is

$$
\begin{aligned}
u_{k,n}(p) = u_{k,n}(\hat{P}) &- \sum_{m=1}^{M}\sum_{\alpha=13}^{27}\left[\oint_{Lm}(\overline{\sigma}_{\alpha ij}(\hat{\mathbf{z}})U_{ik}(\mathbf{z}) - \overline{u}_{\alpha i}(\hat{\mathbf{z}})\Sigma_{ijk}(\mathbf{z}))\epsilon_{jnt}\,\mathrm{d}z_t\right]\left[\overset{m}{T}{}^{-1}\overset{m}{a}\right]_{\alpha} \\
&+ \sum_{m=1}^{M}\sum_{\alpha=4}^{12}\left[\oint_{Lm}(\overline{\sigma}_{\alpha ij}(\mathbf{z})U_{ik}(\mathbf{z}) - \overline{u}_{\alpha i}(\mathbf{z})\Sigma_{ijk}(\mathbf{z}))\epsilon_{jst}z_s\,\mathrm{d}z_t\right]\left[R_{,n}(p)\overset{m}{T}{}^{-1}\overset{m}{a}\right]_{\alpha-3} \\
&- \sum_{\substack{m=1\\ m\notin S}}^{M}\sum_{\alpha=4}^{12}\left[\oint_{Lm}(\overline{\sigma}_{\alpha ij}(\hat{\mathbf{z}})U_{ik}(\mathbf{z}) - \overline{u}_{\alpha i}(\hat{\mathbf{z}})\Sigma_{ijk}(\mathbf{z}))\epsilon_{jnt}\,\mathrm{d}z_t\right]\left[R(\hat{P})\left(\overset{m}{T}{}^{-1}\overset{m}{a} - \beta\hat{P}\right)\right]_{\alpha-3} \\
&+ \sum_{m=1}^{M}\sum_{\alpha=1}^{3}\left[\oint_{Lm}D_{\alpha jk}(\mathbf{z})\,\mathrm{d}z_j\right]\left[S_{,n}(p)\overset{m}{T}{}^{-1}\overset{m}{a} - S_{,n}(\hat{P})\beta^{\hat{P}}\right]_{\alpha} \\
&+ \sum_{\substack{m=1\\ m\notin S}}^{M}\sum_{\alpha=1}^{3}\left[\oint_{Lm}\Sigma_{\alpha jk}(\mathbf{z})\epsilon_{jnt}\,\mathrm{d}z_t\right]\left[S(\hat{P})\overset{m}{T}{}^{-1}\overset{m}{a} - \beta^{\hat{P}}\right]_{\alpha}.
\end{aligned}
\tag{28}
$$

It should be noted that the first, third and fifth terms, with summations and integrals, on the right-hand side of Eq. (28), arise from the first integral in Eq. (25), whereas, the second and fourth arise from the second integral in Eq. (25). Again, as in the case of Eq. (21), the last but one term on the right-hand side of Eq. (28) is "nearly weakly singular" ($\mathrm{O}(1/r(p,\hat{P}))$ as $Q \to \hat{P}$).

## 4. Nearly singular integrals in the BNM

### 4.1. Displacements at internal points close to the boundary

#### 4.1.1. MLS interpolants

It is assumed that, for 3-D problems, the bounding surface $\partial B$ of a solid body is the union of piecewise smooth segments called panels. One each panel, one defines surface curvilinear coordinates $(s_1, s_2)$. For 3-D linear elasticity, for each component of the displacement vector $\mathbf{u}$ and traction vector $\boldsymbol{\tau}$ on $\partial B$, one defines (Chati et al., 1999):

$$u(\mathbf{s}) = \sum_{i=1}^{m} p_i(\mathbf{s} - \mathbf{s}^E)a_i = \mathbf{p}^{\mathrm{T}}(\mathbf{s} - \mathbf{s}^E)\mathbf{a}, \tag{29}$$

$$\tau(\mathbf{s}) = \sum_{i=1}^{m} p_i(\mathbf{s} - \mathbf{s}^E)b_i = \mathbf{p}^{\mathrm{T}}(\mathbf{s} - \mathbf{s}^E)\mathbf{b}. \tag{30}$$

The monomials $p_i$ (see below) are evaluated in local coordinates $(s_1 - s_1^E, s_2 - s_2^E)$, where $(s_1^E, s_2^E)$, are the global coordinates of an evaluation point $E$. It is important to state here that $a_i$ and $b_i$ are not constants. Their functional dependencies are determined later. The integer $m$ is the number of monomials in the basis used for $u$ and $\tau$. Quadratic interpolants, for example, are the form:

$$\mathbf{p}^{\mathrm{T}}(\tilde{s}_1, \tilde{s}_2) = [1, \tilde{s}_1, \tilde{s}_2, \tilde{s}_1^2, \tilde{s}_2^2, \tilde{s}_1\tilde{s}_2], \quad m = 6, \tag{31}$$

where $\tilde{s}_i = s_i - s_i^E; \quad i = 1, 2.$

The coefficients $a_i$ and $b_i$ are obtained by minimizing the weighted discrete $L_2$ norms:

$$R_u = \sum_{I=1}^{n} w(d_I)\left[\mathbf{p}^{\mathrm{T}}(\mathbf{s}^I - \mathbf{s}^E)\mathbf{a} - \hat{u}_I\right]^2, \tag{32}$$

$$R_\tau = \sum_{I=1}^{n} w(d_I)\left[\mathbf{p}^{\mathrm{T}}(\mathbf{s}^I - \mathbf{s}^E)\mathbf{b} - \hat{\tau}_I\right]^2, \tag{33}$$

where the summation is carried out over the $n$ boundary nodes for which the weight function $w(d_I) \neq 0$ (weight functions are defined in the next subsection of this article). The quantity $d_I = g(\mathbf{s}, \mathbf{s}_I)$ is the length of the geodesic on $\partial B$ between $\mathbf{s}$ and $\mathbf{s}^I$ and these $n$ nodes are said to be within the domain of dependence of a point $\mathbf{s}$ (evaluation point $E$ in Fig. 4). Also, $(s_1^I - s_1^E, s_2^I - s_2^E)$ are the local surface coordinates of the boundary nodes with respect to the evaluation point $s^E = (s_1^E, s_2^E)$ and $\hat{u}_I$ and $\hat{\tau}_I$ are the approximations to the nodal values $u_I$ and $\tau_I$. These equations above can rewritten in compact form as:

$$R_u = (\mathbf{P}(\mathbf{s}^I - \mathbf{s}^E)\mathbf{a} - \hat{\mathbf{u}})^{\mathrm{T}}\mathbf{W}(\mathbf{s}, \mathbf{s}^I)(\mathbf{P}(\mathbf{s}^I - \mathbf{s}^E)\mathbf{a} - \hat{\mathbf{u}}), \tag{34}$$

$$R_\tau = (\mathbf{P}(\mathbf{s}^I - \mathbf{s}^E)\mathbf{b} - \hat{\boldsymbol{\tau}})^{\mathrm{T}}\mathbf{W}(\mathbf{s}, \mathbf{s}^I)(\mathbf{P}(\mathbf{s}^I - \mathbf{s}^E)\mathbf{b} - \hat{\boldsymbol{\tau}}), \tag{35}$$

where $\hat{\mathbf{u}}^{\mathrm{T}} = (\hat{u}_1, \hat{u}_2, \ldots, \hat{u}_n)$, $\hat{\boldsymbol{\tau}}^{\mathrm{T}} = (\hat{\tau}_1, \hat{\tau}_2, \ldots, \hat{\tau}_n)$, $\mathbf{P}(\mathbf{s}^I)$ is an $n \times m$ matrix whose $k$th row is:

$$[1, p_2(s_1^k, s_2^k), \ldots, p_m(s_1^k, s_2^k)],$$

and $\mathbf{W}$ is an $n \times n$ diagonal matrix with $w_{kk} = w(d_k)$ ( no sum over $k$).

The stationarity of $R_u$ and $R_t$, with respect to $\mathbf{a}$ and $\mathbf{b}$, respectively, leads to the equations:

$$\mathbf{a}(\mathbf{s}) = \mathbf{A}^{-1}(\mathbf{s})\mathbf{B}(\mathbf{s})\hat{\mathbf{u}}, \quad \mathbf{b}(\mathbf{s}) = \mathbf{A}^{-1}(\mathbf{s})\mathbf{B}(\mathbf{s})\hat{\boldsymbol{\tau}}, \tag{36}$$

where

$$\mathbf{A}(\mathbf{s}) = \mathbf{P}^{\mathrm{T}}(\mathbf{s}^I - \mathbf{s}^E)\mathbf{W}(\mathbf{s}, \mathbf{s}^I)\mathbf{P}(\mathbf{s}^I - \mathbf{s}^E), \quad \mathbf{B}(\mathbf{s}) = \mathbf{P}^{\mathrm{T}}(\mathbf{s}^I - \mathbf{s}^E)\mathbf{W}(\mathbf{s}, \mathbf{s}^I). \tag{37}$$

It is noted from above that the coefficients $a_i$ and $b_i$ turn out to be functions of $\mathbf{s}$. Substituting Eq. (36) into Eqs. (29) and (30) leads to

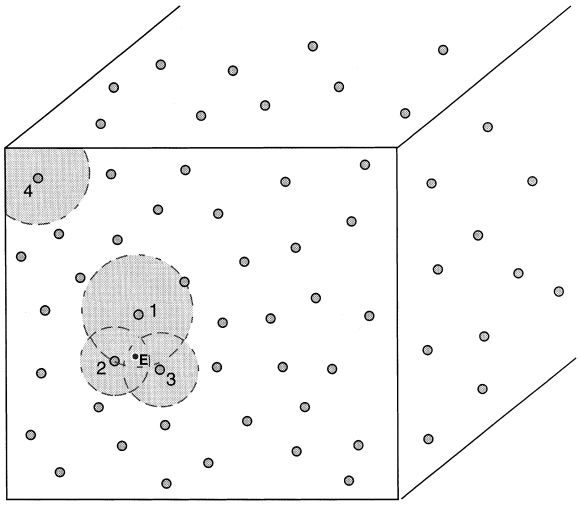


Fig. 4. Nodes 1, 2 and 3 lie within the domain of dependence of $E$. The range of influence of 4 is truncated at the edges of the body.

$$u(\mathbf{s}) = \sum_{I=1}^{n} \Phi_I(\mathbf{s})\hat{u}_I, \quad \boldsymbol{\tau}(\mathbf{s}) = \sum_{I=1}^{n} \Phi_I(\mathbf{s})\hat{T}_I, \tag{38}$$

where the interpolating functions $\Phi_I$ are:

$$\Phi_I(\mathbf{s}) = \sum_{j=1}^{m} p_j(\mathbf{s} - \mathbf{s}^E)(\mathbf{A}^{-1}\mathbf{B})_{jI}(\mathbf{s}). \tag{39}$$

As mentioned previously, $\hat{\mathbf{u}}$ and $\hat{\boldsymbol{\tau}}$ are approximations to the actual nodal values $\mathbf{u}$ and $\boldsymbol{\tau}$. The two sets of values can be related by finding the number of nodes in the range of influence of each collocation node and then evaluating the interpolating function at each of these nodes. Thus, carrying out this procedure for each of the collocation nodes, one gets

$$[\mathbf{H}]\{\hat{\mathbf{u}}_k\} = \{\mathbf{u}_k\}, \quad [\mathbf{H}]\{\hat{\boldsymbol{\tau}}_k\} = \{\boldsymbol{\tau}_k\}, \qquad k = 1, 2, 3. \tag{40}$$

Eqs. (40) relate the nodal approximations of the displacement and traction to their actual nodal values.

#### 4.1.2. Weight functions

The basic idea behind the choice of a weight function is that its value should decrease with distance from a node and that it should have compact support so that the region of influence of the node (see Fig. 4) is of finite extent. A possible choice is the Gaussian weight function

$$w(d) = \begin{cases} \mathrm{e}^{-(d/\hat{c})^2} & \text{for } d \leqslant 1, \\ 0 & \text{for } d > 1, \end{cases} \tag{41}$$

where $d = d_I/\hat{d}_I = g(\mathbf{s}, \mathbf{s}^{\mathbf{I}})/\hat{d}_I$ and $\hat{c}$ is a constant. Here $d_I$ is the *minimum distance*, measured on the surface $\partial B$, (i.e. the geodesic) between a point $\mathbf{s}$ and the collocation node $I$. In the research performed to date, the region of influence of a node has been truncated at the edge of a panel (Fig. 4) so that geodesics (and their derivatives that are required for the stress BNM) need only be computed on piecewise smooth surfaces. Finally, the quantities $\hat{d}_I$ or can be adjusted such that approximately the same number of nodes get included in the domain of dependence of any evaluation point $E$. Both these ideas have been successfully implemented by Mukherjee's group (Chati and Mukherjee, in press; Chati et al., 1999, 2000).

#### 4.1.3. Coupling of the BIE with MLS interpolants

MLS interpolants must be coupled with the continuous BIE (Eq. (4)) in order to create the continuous BNM equation. Substituting the MLS interpolations of $\mathbf{u}$ and $\boldsymbol{\tau}$ from Eq. (38) into Eq. (4), and dividing the bounding surface $\partial B$ into $N_c$ cells, one gets

$$u_k(p) = u_k(\hat{P}) + \sum_{m=1}^{N_c} \int_{\partial B_m} \left[ U_{ik}(p, Q) \sum_{I=1}^{n_Q} \Phi_1(Q)\hat{\tau}_{iI} - T_{ik}(p, Q) \left\{ \sum_{I=1}^{n_Q} \Phi_I(Q)\hat{u}_{iI} - u_i(\hat{P}) \right\} \right] \mathrm{d}S(Q), \tag{42}$$

where $\Phi_I(Q)$ are the contributions from the $I$th node to the field point $Q$. Also, $n_Q$ nodes lie in the domain of dependence of the field point $Q$. The cells, which can be flat or curved, are needed for integration only. They need not be compatible, in the sense that a given cell can be subdivided without affecting its neighbors in any way. The geometry of a cell is interpolated in the usual way, such as with Q4 or T6 elements.

### 4.2. Stresses at internal points close to the boundary

The stress BIE (Eq. (9)) requires the displacement gradients and stresses at the target point $\hat{P}$ (in addition to the usual displacements and tractions at field points $Q$). Displacement gradients on the surface of the body are obtained as part of the BNM solution of the original boundary value problem. This procedure, adapted from Lutz et al. (1992) for the BEM, is described in detail in Chati et al. (2000) and is not repeated here in the interest of brevity.

Using Eq. (38), the BNM version of the continuous stress BIE (Eq. (9)) becomes:

$$\sigma_{ij}(p) = \sigma_{ij}(\hat{P}) + \int_{\partial B} D_{ijk}(p,Q)\left[\sum_{I=1}^{n_Q} \Phi_I(Q)\hat{\tau}_{kI} - \sigma_{km}(\hat{P})n_m(Q)\right] \mathrm{d}S(Q) - \int_{\partial B} S_{ijk}(p,Q)\left[\sum_{I=1}^{n_Q} \Phi_I(Q)\hat{u}_{kI} - u_k(\hat{P}) - u_{k,\ell}(\hat{P})(y_\ell(Q) - x_\ell(\hat{P}))\right] \mathrm{d}S(Q). \tag{43}$$

It should be mentioned here that, for comparison purposes, numerical results are also presented in the next section from the *standard* BNM. For this purpose, BNM versions of the BEM Eqs. (2) and (7) are derived in analogous fashion.

## 5. Numerical results

The sample problem considered here is that of a hollow sphere subjected to internal pressure. The chosen sphere has inner and outer radii $a$ and $b$ equal to 1 and 4 units, respectively. The internal pressure is 1 unit. The elastic constant are Young's modulus $E = 1$ and Poisson's ratio $v = 0.25$, respectively. Numerical results for internal displacement and stresses, from the *standard* as well as *new* BCM and BNM formulations, are compared with exact solutions for this problem.

### 5.1. Boundary contour method results

#### 5.1.1. Mesh

One-eighth of the hollow sphere is modeled here. The boundary elements are curved triangular CIM-9 elements described in Mukherjee et al. (1997). Sixty four elements are used on each of the five (two curved and three flat) faces of the one-eighth sphere–for a total of 320 elements. A generic mesh of this type is shown in Mukherjee et al. (1998).

#### 5.1.2. Internal displacement and stresses

The radial displacement, at internal points along a radius of the hollow sphere, from the *standard* and *new* BCM methods, are compared with the exact solution (Timoshenko and Goodier, 1970) in Fig. 5. Enlarged details, corresponding to the left and right ends of the curve, appear in Figs. 6 and 7, respectively. The results from the *new* BCM (Eq. (21)) are seen to be very accurate everywhere, while those from the *standard* BCM (Eq. (18)) exhibit significant errors near the inner and outer surfaces of the sphere.

Similiar results from the *new* BCM (Eq. 28), for the radial and circumferential stresses as functions of radius, are compared with the exact solutions in Fig. 8. Corresponding results from the *standard* BCM

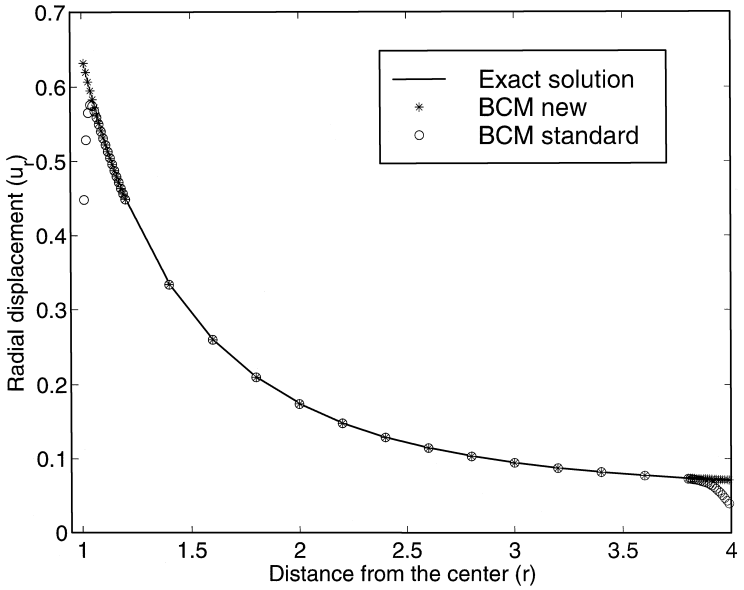


Fig. 5. Radial displacement as a function of radius from the *new* and *standard* BCMs, together with the exact solution.

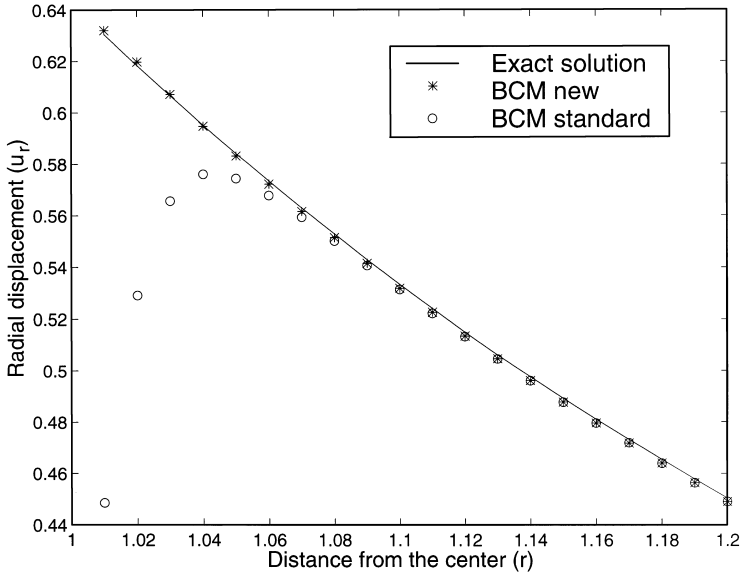


Fig. 6. Radial displacement as a function of radius from the *new* and *standard* BCMs, together with the exact solution, for points *very close* to the inner surface.

(Eq. (24)), at internal points near the inner surface of the sphere, appear in Fig. 9 (radial stress $\sigma_{rr}$ and Fig. 10 (circumferential stress $\sigma_{\theta\theta}$), respectively. Numerical results from the *standard* BCM exhibit large errors (see Figs. 9 and 10), whereas results from the *new* BCM faithfully track the exact solutions in both cases.

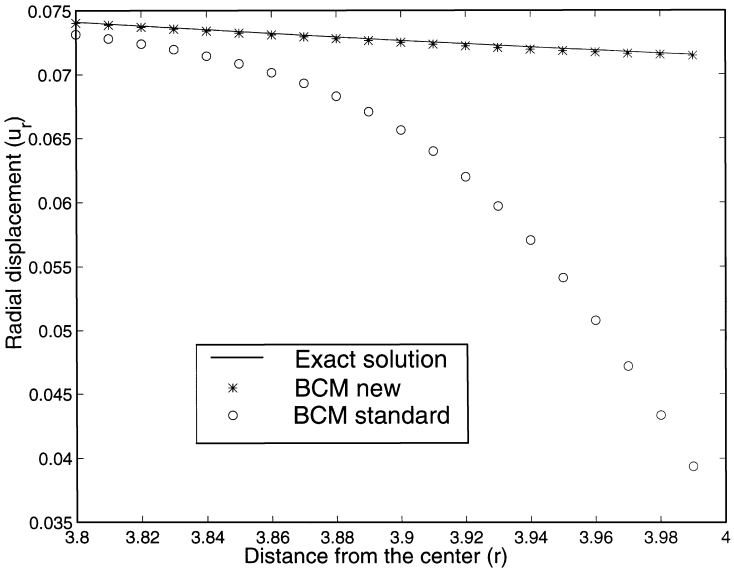


Fig. 7. Radial displacement as a function of radius from the *new* and *standard* BCMs, together with the exact solution, for points *very close* to the outer surface.

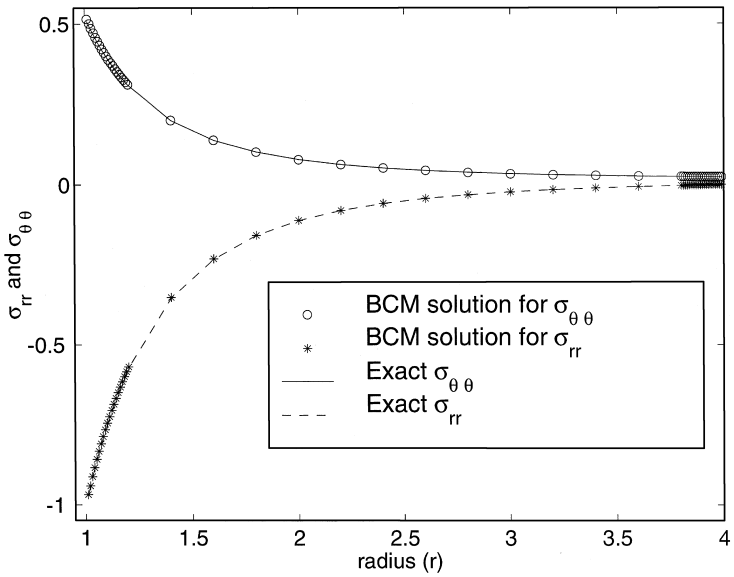


Fig. 8. Radial and circumferential stresses as functions of radius, from the *new* BCM, together with exact solutions.

## 5.2. Boundary node method results

### 5.2.1. Cell configuration

The entire hollow sphere is modeled in this case. 72 quadratic $T6$ triangles are used on each surface of the hollow sphere, together with one cetroidal node per triangle. Further details are available in Chati et al. (1999).

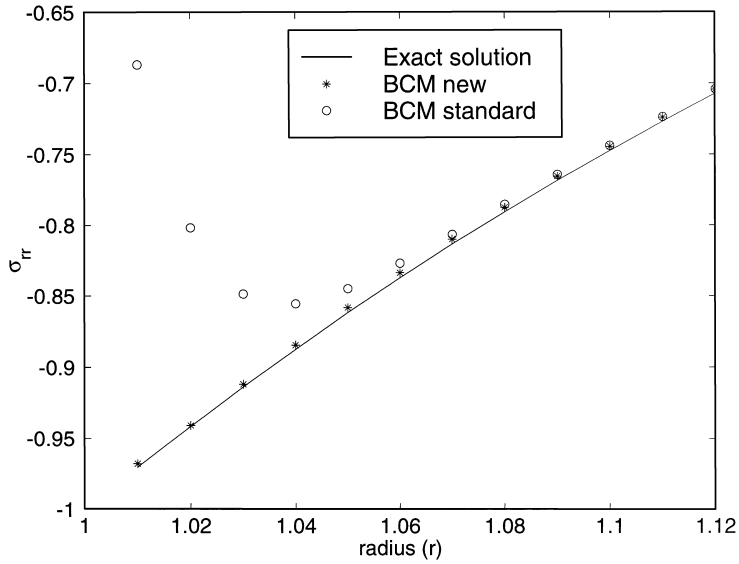


Fig. 9. Radial stress $\sigma_{rr}$ as a function of radius, from the *new* and *standard* BCMs, together with the exact solution, for points *very close* to the inner surface.

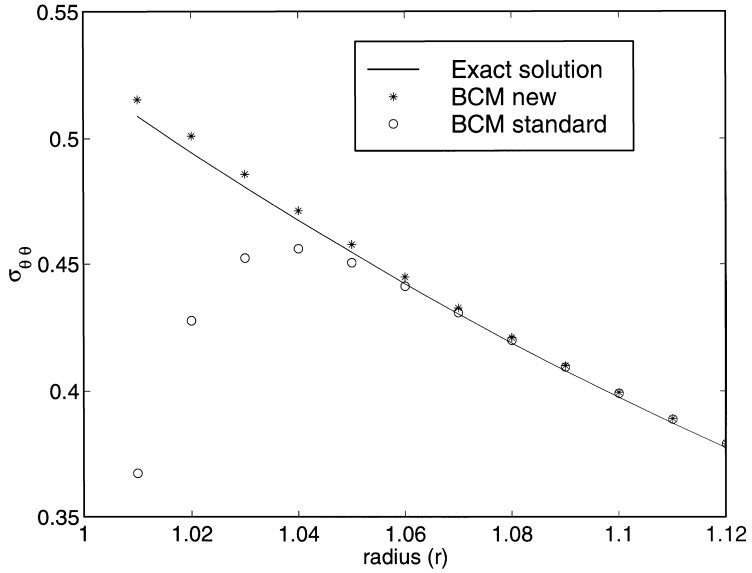


Fig. 10. Circumferential stress $\sigma_{\theta\theta}$ as a function of radius, from the *new* and *standard* BCMs, together with the exact solution, for points *very close* to the inner surface.

### 5.2.2. Internal displacement and stresses

Analogous results from the BNM are presented in Figs. 11–13. The radial displacement, as a function of radius, from the *standard* and *new* BNM methods, are compared with the exact solution of the problem in Fig. 11. Again, the results from the *new* method are very accurate at all the internal points at which these

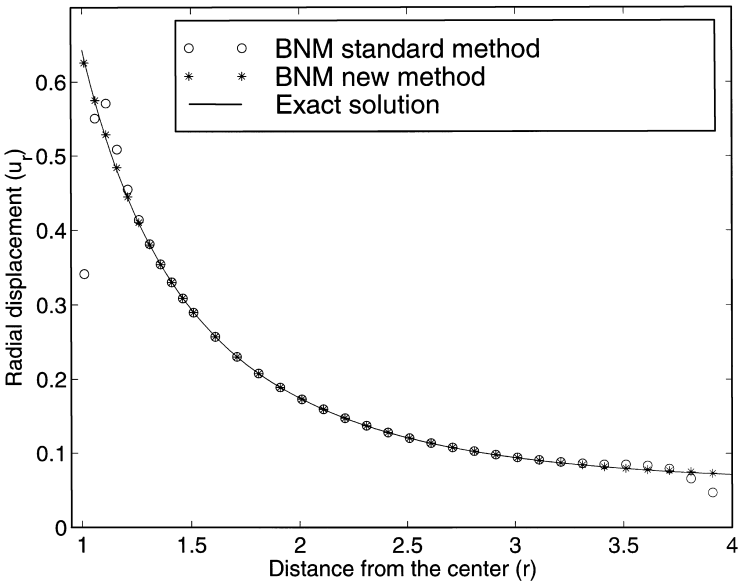


Fig. 11. Radial displacement as a function of radius from the *new* and *standard* BNMs, together with the exact solution.

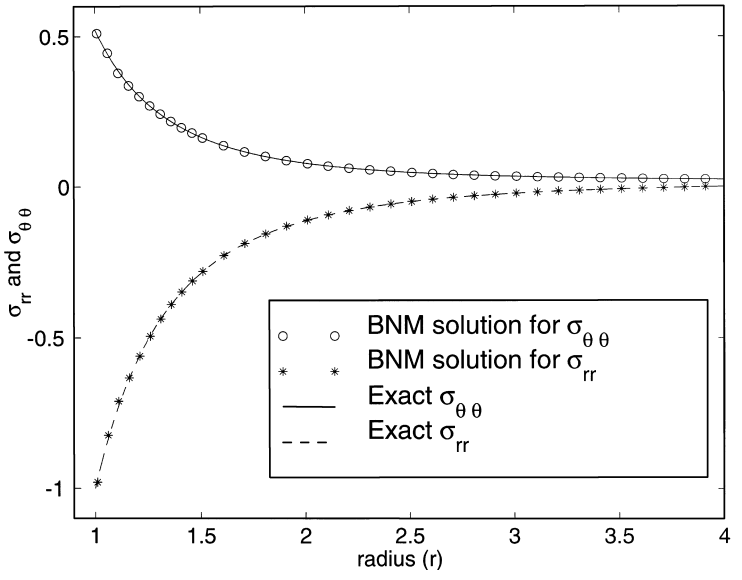


Fig. 12. Radial and circumferential stresses as functions of radius, from the *new* BNM, together with the exact solutions.

results have been calculated, whereas the results from the *standard* approach exhibit large errors near the inner surface of the sphere and some errors near the outer surface.

The radial and circumferential stresses, from the *new* BNM Eq. (43) are compared with the exact solution in Fig. 12. The agreement between the solutions is excellent throughout, including at points that are *very close* to the boundary. Finally, the stress solutions from the *standard* BNM are also included in Fig. 13.

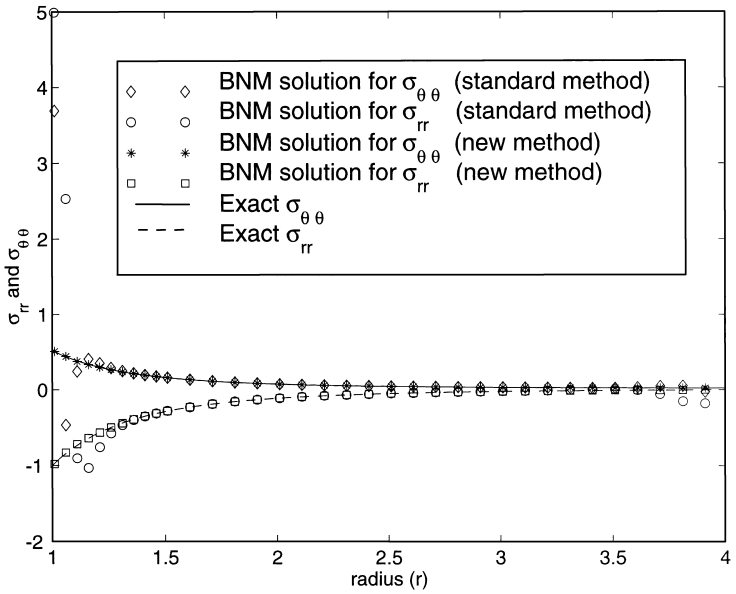


Fig. 13. Radial and circumferential stresses as functions of radius, from the *new* and *standard* BNMs, together with the exact solutions.

Table 1
Radial and circumferential stresses as functions of radius, from the *new* and *standard* BNM, together with the exact solutions, for points *very close* to the inner surface

| Radius ($r$) | $\sigma_{rr}$ | | | $\sigma_{\theta\theta}$ | | |
|---|---|---|---|---|---|---|
| | Standard | New | Exact | Standard | New | Exact |
| 1.01 | 4.99057 | −0.98020 | −0.97012 | 3.68714 | 0.51168 | 0.50887 |
| 1.03 | 5.43126 | −0.92753 | −0.91379 | 1.08215 | 0.49365 | 0.48071 |
| 1.05 | 3.76287 | −0.85789 | −0.86168 | −0.35304 | 0.46201 | 0.45465 |
| 1.07 | 1.39290 | −0.79589 | −0.81338 | −0.36737 | 0.42834 | 0.43050 |
| 1.09 | −0.18719 | −0.74915 | −0.76857 | −0.01546 | 0.40084 | 0.40809 |
| 1.11 | −0.90056 | −0.71229 | −0.72693 | 0.24717 | 0.37928 | 0.38727 |

Details near the inner surface of the sphere are presented in Table 1. It is observed that the *standard* BNM stress solutions are meaningless very near the inner surface of the sphere, and an algorithm for improving these results, such as the *new* BNM presented in this article, is absolutely essential in this case.

## 6. Concluding remarks

The primary contribution of this article is the presentation of a *new* algorithm for regularization of nearly singular and nearly hypersingular integrals, that arise when boundary integral equations are employed to calculate displacements and stresses, in linear elasticity, at internal points that are situated near the bounding surface of a bulky body. The idea is first presented in the context of the *standard* BEM, and is then extended to the BCM and the BNM. The proposed method is *very easy* to implement into a *standard*

BEM (or BCM or BNM) computer code. Numerical results for an example problem of a sphere under internal pressure illustrate the power of the *new* method.

The *new* method can be used universally for all internal points, both near and far from the boundary of a bulk body. The method has also been used for the 3-D Laplace's equation in Chati et al. (1999) and can be extended to other problems. This *new* method, which is easily applicable to bulky bodies, complements the elegant approach for thin bodies that has been presented earlier by Liu (1998). It is recommended that the approach presented in this article be routinely employed whenever boundary integral based methods are used to calculate variables at internal points that are *close* to the boundary of a bulky body. This method, in its current form, is not recommended for thin shell problems. It is expected, however, that it can be extended, in future, for use in the analysis of such problems.

**Acknowledgements**

The contributions of Mukherjee and Chati, to this research, have been supported by a University Research Program (URP) grant, from Ford Motor Company, to Cornell University. The contribution of Shi, to this research, has been supported by the NSF SBIR Phase II grant DMI-9629076 to DeHan Engineering Numerics.

## Appendix A. Displacement BIE and stress BIE kernels

The Kelvin kernels for the displacement BIE (1) for 3-D linear elasticity are

$$U_{ik} = \frac{1}{16\pi G(1-\nu)r}[(3-4\nu)\delta_{ik} + r_{,i}\, r_{,k}\,],$$

$$\Sigma_{ijk} = -\frac{1}{8\pi(1-\nu)r^2}[(1-2\nu)(r_{,i}\,\delta_{jk} + r_{,j}\,\delta_{ik} - r_{,k}\,\delta_{ij}) + 3r_{,i}\, r_{,j}\, r_{,k}\,].$$

The traction kernel in Eq. (2) is:

$$T_{ik} = \Sigma_{ijk} n_j = -\frac{1}{8\pi(1-\nu)r^2}\left[\{(1-2\nu)\delta_{ik} + 3r_{,i}\, r_{,k}\}\frac{\partial r}{\partial n} + (1-2\nu)(r_{,i}\, n_k - r_{,k}\, n_i)\right].$$

The corresponding kernels for the stress BIE (7) are:

$$D_{ijk} = E_{ijmn}\frac{\partial U_{km}}{\partial x_n} = \frac{1}{8\pi(1-\nu)r^2}[(1-2\nu)(\delta_{ik}r_{,j} + \delta_{kj}r_{,i} - \delta_{ji}r_{,k}\,) + 3r_{,i}\, r_{,j}\, r_{,k}\,],$$

$$\begin{aligned} S_{ijk} &= E_{ijmn}\frac{\partial T_{km}}{\partial x_n} \\ &= \frac{G}{4\pi(1-\nu)r^3}\left[\{(1-2\nu)\delta_{ij}r_{,k} + \nu(\delta_{ik}r_{,j} + \delta_{jk}r_{,i}\,) - 5r_{,i}\, r_{,j}\, r_{,k}\}3\frac{\partial r}{\partial n} + 3\nu(n_i r_{,j}\, r_{,k} + n_j r_{,k}\, r_{,i}\,)\right. \\ &\quad \left. - (1-4\nu)n_k\delta_{ij} + (1-2\nu)(3n_k r_{,i}\, r_{,j} + n_j\delta_{ki} + n_i\delta_{jk})\right]. \end{aligned}$$

In the above, $r$ is the distance between a source point $\mathbf{x}$ and a field point $\mathbf{y}$, $G$ and $\nu$ are the shear modulus and Poisson's ratio, respectively, $\delta_{ik}$ are the components of the Kronecker delta and, $k \equiv \partial/\partial y_k$. Also, the

components of the normal as well as the normal derivative $\partial r/\partial n$ are evaluated at the field point **y** and $E_{ijmn}$ are components of the elasticity tensor for a homogeneous isotropic elastic solid.

## References


Banerjee, P.K., 1994. The Boundary Element Methods in Engineering, McGraw-Hill, London.

Belytschko, T., Krongauz, Y., Organ, D., Fleming, M., Krysl, P., 1996. Meshless methods: an overview and recent developments. Comput. Methods Appl. Mech. Engng. 139, 3–47.

Chati, M.K., 1999. Meshless Standard and Hypersingular Boundary Node Method – Applications in Three-Dimensional Potential Theory and Linear Elasticity. Ph.D. dissertation, Cornell University, Ithaca, NY.

Chati, M.K., Mukherjee, S. The boundary node method for three-dimensional problems in potential theory. Int. J. Numer. Methods Engng., in press.

Chati, M.K., Mukherjee, S., Mukherjee, Y.X. 1999. The boundary node method for three-dimensional linear elasticity. Int. J. Numer. Methods Engng. 46, 1163–1184.

Chati, M.K., Paulino, G.H., Mukherjee, S., 2000. The meshless standard and hypersingular boundary node methods – applications to error estimation and adaptivity in three-dimensional problems, Submitted for publication.

Cruse, T.A., 1969. Numerical solutions in three-dimensional elastostatics. Int. J. Solids Structures 5, 1259–1274.

Cruse, T.A., Aithal, R., 1993. Non-singular boundary integral equation implementation. Int. J. Numer. Methods Engng. 36, 237–254.

Cruse, T.A., Richardson, J.D., 1996. Non-singular somigliana stress identities in elasticity. Int. J. Numer. Methods Engng. 39, 3273–3304.

Huang, Q., Cruse, T.A., 1993. Some notes on singular integral techniques in boundary element analysis. Int. J. Numer. Methods Engng. 36, 2643–2659.

Krishnasamy, G., Rizzo, F.J., Rudolphi, T.J., Hypersingular boundary integral equations: their occurrence, interpretation, regularization and computation. In: Banerjee, P.K., Kobayashi, S. (Eds.), Development in Boundary Element Methods-7, Elsevier, London, 207–252.

Krishnasamy, G., Rizzo, F.J., Liu, Y.J., 1994. Boundary integral equations for thin bodies. Int. J. Num. Methods Engng. 37, 107–121.

Kothnur, V., Mukherjee, S., Mukherjee, Y.X., 1999. Two-dimensional linear elasticity by the boundary node method. Int. J. Solids Structures 36, 1129–1147.

Liu, Y.J., Zhang, D., Rizzo, F.J., 1993. Nearly singular and hypersingular integrals in the boundary element method. In: Brebbia, C.A., Rencis, J.J. (Eds.), Boundary Elements XV. Computational Mechanics Publication, Southampton, pp. 453–468.

Liu, Y.J., 1998. Analysis of shell-like structures by the boundary element method based on 3-D elasticity: formulation and verification. Int. J. Numer. Methods Engng. 41, 541–558.

Liu, Y.J., Xu, N., Luo, J., 1999. Modeling of interphases in fiber-reinforced composites under transverse loading using the boundary element method, Submitted for publication.

Luo, J.F., Liu, Y.J., Berger, E.J., 1998. Analysis of two-dimensional thin structures from micro- to nano-scales using the boundary element method. Comput. Mech. 22, 404–412.

Lutz, E.D., 1991. Numerical Methods for Hypersingular and Near-Singular Boundary Integrals in Fracture Mechanics. Ph.D. Dissertation, Cornell University, Ithaca, NY.

Lutz, E.D., Ingraffea, A.R., Gray, L.J., 1992. Use of 'simple solutions' for boundary integral methods in elasticity and fracture analysis. Int. J. Numer. Methods Engng. 35, 1737–1751.

Mukherjee, S., 1982. Boundary Element Methods in Creep and Fracture, Elsevier, London.

Mukherjee, Y.X., Mukherjee, S., 1997. The boundary node method for potential problems. Int. J. Numer. Methods Engng. 40, 797–815.

Mukherjee, Y.X., Mukherjee, S., Shi, X., Nagarajan, A., 1997. The boundary contour method for three-dimensional linear elasticity with a new quadratic boundary element. Eng. Anal. Bound. Elem. 20, 35–44.

Mukherjee, S., Mukherjee, Y.X., 1998. The hypersingular boundary contour method for three-dimensional linear elasticity. ASME J. Appl. Mech. 65, 300–309.

Mukherjee, S., Shi, X., Mukherjee, Y.X., 1998. Surface variables and their sensitivities for three-dimensional linear elasticity by the boundary contour method. Comput. Methods Appl. Mech. Engng. 173, 387–402.

Mukherjee, S., Shi, X., Mukherjee, Y.X. Internal variables and their sensitivities in three-dimensional linear elasticity by the boundary contour method. Comput. Methods Appl. Mech. Engng., in press.

Nagarajan, A., Lutz, E.D., Mukherjee, S., 1994. A novel boundary element method for linear elasticity with no numerical integration for 2-D and line integrals for 3-D problems. ASME J. Appl. Mech. 61, 264–269.

Nagarajan, A., Mukherjee, S., Lutz, E.D., 1996. The boundary contour method for three-dimensional linear elasticity. ASME J. Appl. Mech. 63, 278–286.

Nakagawa, N., 1993. Near-surface field evaluation in two-phase Helmholtz problem. IABEM-93 Symposium, Braunschweig, Germany.

Phan, A.-V., Mukherjee, S., Mayer, J.R.R., 1997. The boundary contour method for two-dimensional linear elasticity with quadratic boundary elements. Comput. Mech. 20, 310–319.

Phan, A.-V., Mukherjee, S., Mayer, J.R.R., 1998. The hypersingular boundary contour method for two-dimensional linear elasticity. Acta Mech. 130, 209–225.

Rizzo, F.J., 1967. An integral equation approach to boundary value problems of classical elastostatics. Qly. Appl. Math. 25, 83–95.

Rudolphi, T.J., 1991. The use of simple solutions in the regularization of hypersingular boundary integral equations. Math. Comput. Model. 15, 269–278.

Timoshenko, S.P., Goodier, J.N., 1970. Theory of Elasticity, Third edn. McGraw-Hill, New York.